Optical Properties of 4-Bromobenzaldehyde Derivatives in Chloroform Solution

ARTICLE *in* THE JOURNAL OF PHYSICAL CHEMISTRY A · AUGUST 2014

Impact Factor: 2.69 · DOI: 10.1021/jp505411r · Source: PubMed

THE JOURNAL OF PHYSICAL CHEMISTRY A

Article

pubs.acs.org/JPCA

Optical Properties of 4-Bromobenzaldehyde Derivatives in Chloroform Solution

Clàudia Climent,[†] Pere Alemany,[†] Dongwook Lee,[‡] Jinsang Kim,[‡] and David Casanova*[,§,¶]

[†]Departament de Química Física and Institut de Química Teòrica i Computacional (IQTCUB), Universitat de Barcelona, Martí i Franquès, 1-11, 08028 Barcelona, Spain

[‡]Materials Science and Engineering, Macromolecular Science and Engineering, Chemical Engineering, and Chemistry, University of Michigan, Ann Arbor, Michigan 48109, United States

[§]Kimika Fakultatea, Euskal Herriko Unibertsitatea (UPV/EHU), Donostia International Physics Center (DIPC), P.K. 1072, 2080 Donostia, Spain

[¶]IKERBASQUE, Basque Foundation for Science, Bilbao, 48011, Spain

Supporting Information

ABSTRACT: In this work we give a deeper insight into the electronic structure of a series of purely organic molecules that were recently employed as building blocks in crystals with very efficient phosphorescent emission. With this purpose, the low-lying excited states of a series of 4-bromobenzaldehyde derivatives in chloroform solution are explored by means of time-dependent density functional theory (TDDFT) calculations, together with the absorption, fluorescence, and phosphorescence experimental spectra. The optical properties of the studied molecular models are extensively discussed, in terms of the frontier molecular orbitals involved in the relevant electronic transitions, the recorded and simulated absorption profiles, and the molecular geometries and transition energies of the emitting states. The calculations eventually help in the assignment of the character of the lowest lying singlet and triplet emitting states for these compounds.

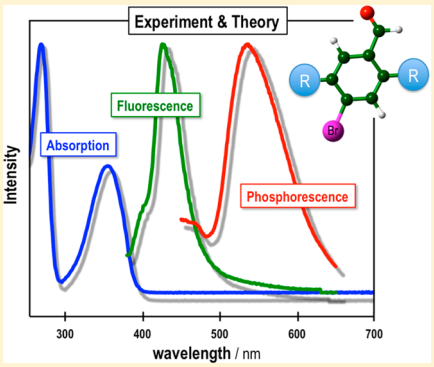

1. INTRODUCTION

The importance of organic electronic devices[1−6] has been steadily increasing over the last two decades, evolving from a research field with great promise for new materials and applications to a real industry with commercial products on the market. In an emerging era of flexible, rollable, or foldable high performance displays, the search for new low-cost, mechanically tolerant functional materials that can be easily processed has become one of the major focuses of interest in material sciences. Organic materials that can be precisely printed, stamped, sprayed, drop-cast, or spin-coated into predefined patterns offer a competitive alternative to their conventional inorganic homologues for applications in thin-film transistors (TFTs), photovoltaic cells, radio frequency identification (RFID) tags, sensors, memories, or light-emitting diodes (LEDs).

Despite the obvious advantage of purely organic materials for these applications, in some cases, the chemical nature of these compounds poses some serious drawbacks for the development of new functional materials for a specific application. This is, for instance, the case of the development of purely organic LEDs (OLEDs) since it is well-known that competitive organic phosphorescent materials are very scarce due to inefficient spin−orbit coupling in compounds containing only light elements, which prevents singlet and triplet mixing. For this reason, during the past decade, much attention has been paid mainly to organometallic materials, such as iridium(III) complexes,[7] because of their enhanced emission capabilities. The presence of a heavy atom, which facilitates intensity borrowing of the lowest triplet state from bright singlet states, has given these organometallic complexes a central role in the field of OLEDs.[8] Despite the fact that organometallic compounds possess the appropriate physical properties as far as light emission is concerned, purely organic compounds present a series of very advantageous features, which make them very attractive for OLED technology. Purely organic molecules are indeed much cheaper and easier to synthesize than their organometallic counterparts and, by fine-tuning their structure, different emission properties can be readily achieved. However, the quantum yield for phosphorescent emission must be highly improved in order for purely organic materials to be able to compete with organometallics in practical applications.

The photophysical properties of a wide family of aromatic carbonyls, such as benzaldehyde and naphthalene derivatives,[9−11] were largely studied decades ago, and different strategies were conducted in order to improve their phosphorescence.[12,13] One of these strategies, known as the heavy atom effect,[14,15] consists in introducing an atom of a

Received: June 2, 2014
Revised: August 11, 2014
Published: August 11, 2014

   dx.doi.org/10.1021/jp505411r | J. Phys. Chem. A 2014, 118, 6914−6921

heavy element such as, for instance, bromine, either directly in the emitting molecular entity or in the solvent with the aim of favoring the phosphorescent emission by enhancing the rate of the spin-forbidden processes. Experimental evidence corroborated that the presence of heavy atoms in halogenonaphthalenes,[16,17] as well as halogenated aromatic carbonyl compounds[18,19] increased very successfully the phosphorescence quantum yields in these compounds. The use of halogenated solvents[16,20] was also shown to produce a systematic intensity increase of the spin-forbidden absorption band of aromatic compounds, with heavier halogen atoms inducing more intense absorption bands. All this knowledge allowed a rationalization of the requisites for enhancing organic phosphorescence, but competition with nonradiative decay processes was still found to be a major drawback, and no really efficient purely organic phosphorescent materials to be used in real technological applications could be developed.

It was not until three years ago that efficient phosphorescence was reported by one of our groups for purely organic crystalline materials,[21] with an excellent phosphorescence quantum yield of 55% at room temperature in practical ambient conditions. The basic building block for those crystals was 2,5-dihexyloxy-4-bromobenzaldehyde (Br6A in Scheme 1) although other directed heavy atom phosphors with substitutions in the aromatic ring, that is, BrC6A, BrS6A, and Np6A in Scheme 1, were also studied.

Scheme 1. Studied 4-Bromobenzaldehyde Molecules

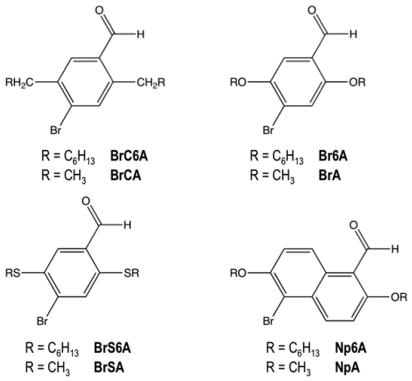

The emission spectrum of Br6A in chloroform solution only showed a fluorescence band at room temperature, while phosphorescence emission was only detected at 77 K. On the other hand, crystalline samples exhibited strong phosphorescence and weaker fluorescence bands, clearly indicating that halogen bonding in the crystals is essential for efficient solid-state phosphorescent emission to take place. When halogen bonding comes to play, electrons from the carbonyl oxygen atom are partially delocalized onto the bromine of a neighboring molecule, resulting in very efficient spin−orbit coupling, which promotes intersystem crossing that can now compete with fluorescence. This rapid population of the lowest triplet state results in a decrease in the intensity of fluorescence and, together with the suppression of the vibrational loss of triplets in the solid state, efficient phosphorescence is observed.

The aim of the present work is to perform a thorough experimental and theoretical study of the photophysical properties of the molecules in solution shown in Scheme 1, to gain some knowledge on the principal features of the molecular radiative processes involving the singlet and triplet $\pi\pi^*$ and $n\pi^*$ states responsible for the UV/vis absorption, fluorescence, and phosphorescence spectra.

2. MATERIALS AND METHODS

A series of bromobenzaldehyde molecules were synthesized according to the previous report.[21] Each molecule was dissolved in chloroform and diluted to 10^{-5} M before measurement. UV−visible absorption spectra were measured at room temperature by using a Varian Cary 50 Bio UV−vis spectrophotometer. Photoluminescent excitation and emission spectra were collected on a Photon Technologies International (PTI) QuantaMaster equipped with a Dewar flask at room temperature and 77 K, respectively.

3. COMPUTATIONAL DETAILS

Although the presence of side hydrocarbon chains in the studied chromophores has an important structural effect, decisively influencing their common crystal packing, they are expected to play, at best, a marginal role in the photophysical properties in solution. Therefore, to reduce the computational cost of the present study, we have replaced the hydrocarbon lateral chains with methyl groups. The molecular models employed for the computational study will be labeled as BrCA, BrA, BrSA, and NpA (Scheme 1) to distinguish them from the compounds for which the actual spectra have been recorded (BrC6A, Br6A, BrS6A, and Np6A). The core of the present computational study relies on density functional theory (DFT) and in particular its time-dependent version (TDDFT), which has shown excellent performance in the computation of spectroscopic properties for a multitude of similar molecular systems,[22−27] in conjunction with the use of continuum solvation models to take into account the solvent environment.[28,29]

Ground-state geometry optimizations were carried out within the framework of DFT, with the B3LYP functional and the Ahlrichs pVDZ basis set.[30] Excited state geometry optimizations were done using TDDFT with the same functional and basis set. We performed frequency analysis for all ground and excited state optimized geometries. In most of the cases we found one or two imaginary frequencies with very small amplitudes (in the order of tens to ∼100 cm^{-1}) corresponding to energetically flat internal rotations mainly located in the methyl lateral groups. Therefore, we are confident that the obtained geometries fairly represent the equilibrium molecular structures for the studied electronic states and that the presence of these low imaginary frequencies does not affect the results of our analysis. The complete list of these frequencies and their characterization is presented as Supporting Information. All calculations regarding geometry optimizations were performed with the Q-Chem package, version 4.0.1.[31] Vertical excitation energies were computed with one-component TDDFT methodology, as implemented in the ADF program,[32−34] introducing scalar relativistic effects via the zero order regular approximation (ZORA) formalism,[35] while spin−orbit coupling was included perturbatively.[36] The B3LYP functional was also used in the calculations of vertical excitation energies to the low-lying singlet and triplet excited states, together with a TZ2P basis set.[37]

Solvent effects were included via the COSMO solvation model[38,39] taking chloroform as the solvent (ε = 4.8). Geometry optimization calculations were performed considering equilibrium of the solvent, while vertical excitations and de-

dx.doi.org/10.1021/jp505411r | J. Phys. Chem. A 2014, 118, 6914−6921

excitations were treated by disregarding the reorganization of the solvent, that is, nonequilibrium approach, using the squared refractive index as the optical dielectric constant for chloroform (ε_{NEq} = 2.09). Transition energies at the ground and excited state geometries were obtained within the linear response (LR) approach. The LR-COSMO energies have been compared to the LR[40,41] and state specific (SS)[42,43] version of the Polarization Continuum Model (PCM).[44] The results show no major differences between the three models and can be found as Supporting Information. All PCM calculations included in the Supporting Information were performed at the B3LYP/pVDZ level with the Gaussian 09 program.[45]

We have tested the dependency of our results on the quality of the basis set by comparing the optimized geometries obtained with pVDZ and Def2-TZVP,[46] and the excitation energies with TZ2P and ATZ2P[47] for the BrA case. The results show very small discrepancies between basis sets, with bond length differences never larger than 0.01 Å, and slightly lower excitation energies when computed with the larger basis (ATZ2P). The numerical values for the comparisons can be found as Supporting Information.

The UV/vis absorption spectra for the four model compounds were simulated with TDDFT calculations. For the lowest 50 singlet and triplet spin pure scalar-relativistic states, spin−orbit coupling was included perturbatively yielding 200 spin−orbit coupled states. The intensity of the simulated spectra has been scaled to match the highest experimental absorption peak, and with a 4000 cm^{-1} half-bandwidth for all transitions. We would like to stress that the calculations do not include vibronic couplings, which might modify the profiles of the simulated absorption spectra.

4. RESULTS AND DISCUSSION

Lowest $\pi\pi^*$ and $n\pi^*$ Excited States. From a qualitative point of view, the main features of the electronic structure of aromatic carbonyls can be described as the result of bonding, antibonding, and nonbonding combinations between the molecular orbitals of a carbonyl group and those of the aromatic ring. The block of the highest lying occupied molecular orbitals (HOMOs) is formed mainly from bonding and/or antibonding combinations of occupied π-orbitals of the conjugated ring with the π and π^* orbitals of the carbonyl group. On the other hand, the block of lowest lying unoccupied orbitals (LUMOs) can be described as bonding combinations of π^*-orbitals from the two fragments. As a result, these molecules exhibit several π and π^* frontier orbitals with various relative energies depending on the substitution of the aromatic ring. Typically, the doubly occupied oxygen lone pair (n) appears within the energy range of the π set from which it can be clearly distinguished since its interaction with the π-system on the aromatic fragment is forbidden by symmetry.

In the present compounds, we expect the presence of two high-energy occupied π-orbitals, that is, the e_{1g} pair in benzene, as the HOMOs, with an energy splitting that depends on the ring substitution pattern that is considered. This is the case of BrCA, BrA, and BrSA molecules, while the naphthalene pattern in NpA, holding a larger conjugated system, results in three occupied π-orbitals in the HOMOs block (see Figure 1, orbitals in green). The S p_z orbitals in the thiomethoxy groups of BrSA are energetically higher than the O p_z orbitals in the methoxy group. As a consequence, DFT calculations on the BrSA molecular model locate an additional π-orbital with important participation of the S p_z atomic orbital between the two

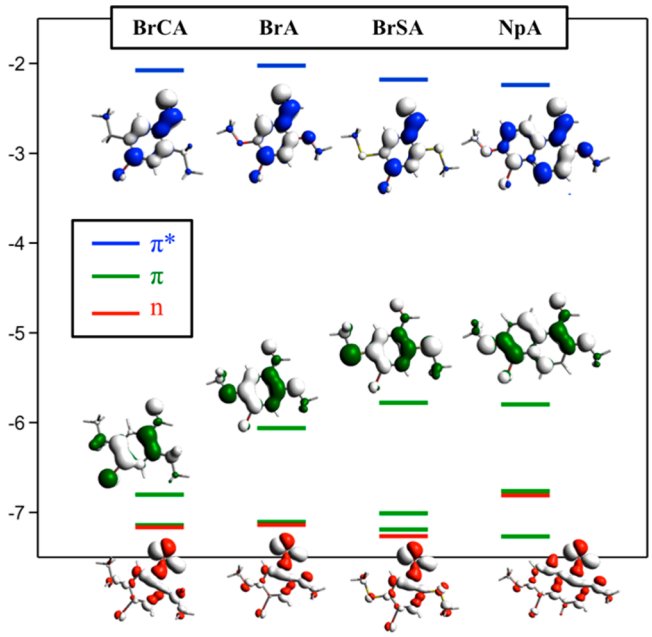

Figure 1. Frontier molecular orbital diagram of BrCA, BrA, BrSA, and NpA model molecules.

conjugated orbitals from the ring (the HOMO-1). Antibonding interactions between the methoxy, thiomethoxy groups as well as the Br atom with the conjugated system of the aromatic ring in BrA, BrSA, and NpA result in a rather large separation between the two highest occupied π-orbitals. On the other hand, due to the C sp^3 substitution, this effect is much less pronounced in BrCA, and the HOMO is 0.7−1.0 eV lower than in the other three cases. The n orbital (Figure 1, orbitals in red) appears at virtually the same energy as the second highest occupied π-orbital of the ring. The energy of n is very similar in BrCA, BrA, and BrSA, while it is 0.3−0.4 eV higher in energy in NpA due to the presence of additional antibonding interactions. In these compounds, the LUMO corresponds to the bonding interaction between the π^* orbital from the carbonyl group and that from the aromatic ring. There is almost no difference both in the topology and the energy of the LUMO (Figure 1, orbitals in blue) in all four molecules. The tiny energy decrease along the BrA > BrCA > BrSA > NpA series can be attributed to an increase of the effective conjugation with the exception of BrCA. This effect also explains the relative energies of the HOMOs (see Results and Discussion in the previous section).

The lowest singlet and triplet states of BrCA, BrA, BrSA, and NpA can be qualitatively described as single-electron transitions from the π and n orbitals to the lowest unoccupied π^* orbital. The relative energies of the n and π orbitals dictate the state ordering in each case, $\pi\pi^*$ states below $n\pi^*$ ones, with the exception of BrCA, where the $^1n\pi^*$ state is 0.44 eV below the $^1\pi\pi^*$ one (Figure 2 and Table 1). The energy difference between excited singlet and triplet states with the same character (ΔE_{ST}) is, to a good approximation, proportional to the overlap between the orbitals involved in the transition. Therefore, $\pi\pi^*$ states present larger ΔE_{ST} values than $n\pi^*$ states. Transition energies to $^3\pi\pi^*$ for the four molecules present the inverse energy ordering obtained for the π HOMO, that is BrCA ≫ BrA > BrSA > NpA. Excitations to the singlet counterparts follow basically the same trend, but the larger localization of the HOMO in BrSA reduces the $\pi-\pi^*$ exchange interaction, and the computed transition energy is ∼0.15 eV

dx.doi.org/10.1021/jp505411r | J. Phys. Chem. A 2014, 118, 6914−6921

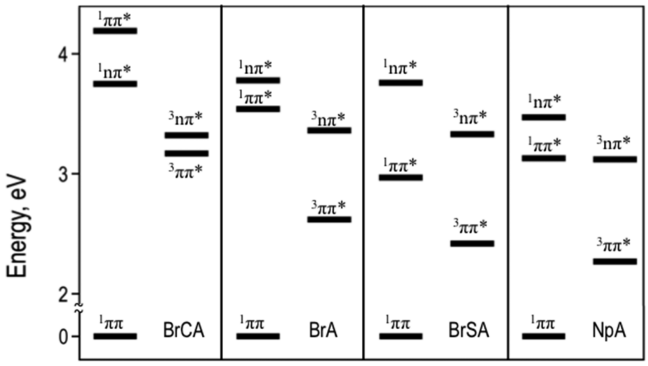

Figure 2. Energy diagram showing the vertical relative energy of the lowest $^{1,3}\pi\pi^*$ and $^{1,3}n\pi^*$ states with respect to the ground state ($^1\pi\pi$) for the BrCA, BrA, BrSA, and NpA molecules at the ground state geometry.

lower than in NpA. Excitation to the lowest $n\pi^*$ singlet and triplet states of BrA, BrCA, and BrSA are very close in energy, that is, 3.75−3.78 eV and 3.32−3.36 eV for the singlet and triplet states, respectively. Destabilization of the n orbital in NpA reduces the computed transitions by 0.2−0.3 eV.

The magnitude of the absorption intensity is also rather different depending on the nature of the excitation hole. Owing to the poor spatial overlap between n- and π^*-type orbitals compared to the overlap between π- and π^*-type ones, the computed oscillator strengths for excitations to the $^1n\pi^*$ state are much smaller than the ones corresponding to the $\pi \rightarrow \pi^*$ transition, that is, between 3 and 4 orders of magnitude smaller. Differences in oscillator strengths between the four molecules studied are less important, although delocalization of the π-HOMO over S atoms in BrSA results in lower strength to the $^1\pi\pi^*$ state compared to BrCA, BrA, and NpA.

Absorption Spectra. The UV−vis absorption spectra of the four target molecules are basically the result of low-lying singlet−singlet $\pi \rightarrow \pi^*$ transitions with much lower participation of $n \rightarrow \pi^*$ excitations. These transitions correspond to single-electron promotions from the occupied orbitals in Figure 1 to the π^*-type LUMO. The computed relative energies and transition intensities to the low-lying excited states of the molecular models are in very good agreement with the absorption maxima obtained from the deconvolution of the experimental spectra (Table 1 and Figure 3).

Table 1. Computed Transition Energies (ΔE), Oscillator Strengths, and Composition for the Lowest Singlet and Triplet Excited States for the BrCA, BrA, BrSA, and NpA Molecules Together with the Absorption Maxima (λ_{max}) in the Deconvoluted Experimental Absorption Spectra of BrC6A, Br6A, BrS6A, and Np6A

state	transition character	ΔE eV (nm)	λ_{max} eV (nm)	oscillator strength	composition (%)
			BrCA		
S_1	$n\rightarrow\pi^*$	3.75 (330)		3×10^{-5}	H-2 → L (97)
S_2	$\pi\rightarrow\pi^*$	4.19 (296)	4.15 (299)	1×10^{-1}	H → L (52)/H-1 → L (39)
S_3	$\pi\rightarrow\pi^*$	4.49 (276)	4.63 (268)	5×10^{-1}	H-1 → L (51)/H → L (42)
S_4	$n_{Br}\rightarrow\pi^*$	5.11 (243)		2×10^{-6}	H-3 → L (98)
T_1	$\pi\rightarrow\pi^*$	3.17 (391)		0×10^{0}	H → L (91)
T_2	$n\rightarrow\pi^*$	3.32 (373)		0×10^{0}	H-2 → L (94)
			BrA		
S_1	$\pi\rightarrow\pi^*$	3.54 (350)	3.44 (361)	2×10^{-1}	H → L (92)
S_2	$n\rightarrow\pi^*$	3.78 (328)	3.68 (337)	1×10^{-4}	H-2 → L (96)
S_3	$\pi\rightarrow\pi^*$	4.62 (269)	4.62 (268)	4×10^{-1}	H-1 → L (88)
S_4	$\pi\rightarrow\sigma^*$	4.87 (255)		1×10^{-5}	H → L+1 (99)
T_1	$\pi\rightarrow\pi^*$	2.62 (473)		0×10^{0}	H → L (98)
T_2	$n\rightarrow\pi^*$	3.36 (369)		0×10^{0}	H-2 → L (93)
			BrSA		
S_1	$\pi\rightarrow\pi^*$	2.97 (418)	3.15 (393)	1×10^{-1}	H → L (96)
S_2	$n\rightarrow\pi^*$	3.76 (330)	3.38 (367)	1×10^{-4}	H-3 → L (95)
S_3	$\pi_S\rightarrow\pi^*$	4.02 (308)	3.58 (346)	1×10^{-2}	H-1 → L (95)
S_4	$\pi\rightarrow\pi^*$	4.41 (281)	4.23 (293)	2×10^{-1}	H → L+1 (49)/H-2 → L (43)
S_5	$\pi\rightarrow\sigma^*$	4.42 (281)		3×10^{-3}	H → L+2 (96)
S_6	$\pi\rightarrow\pi^*$	4.74 (262)	4.82 (257)	1×10^{0}	H-2 → L (48)/H → L+1 (42)
T_1	$\pi\rightarrow\pi^*$	2.42 (512)		0×10^{0}	H → L (97)
T_2	$n\rightarrow\pi^*$	3.33 (372)		0×10^{0}	H-3 → L (92)
			NpA		
S_1	$\pi\rightarrow\pi^*$	3.13 (396)	3.11 (399)	2×10^{-1}	H → L (94)
S_2	$n\rightarrow\pi^*$	3.47 (357)	3.35 (370)	1×10^{-4}	H-2 → L (94)
S_3	$\pi\rightarrow\pi^*$	3.87 (321)	3.85 (322)	2×10^{-1}	H-1 → L (86)
S_4	$\pi\rightarrow\pi^*$	4.51 (275)	4.39 (282)	1×10^{-1}	H-3 → L (75)
S_5	$\pi\rightarrow\pi^*$	4.62 (268)		3×10^{-2}	H → L+1 (69)
S_6	$\pi\rightarrow\sigma^*$	4.72 (263)		1×10^{-4}	H → L+3 (97)
S_7	$n_{Br}\rightarrow\pi^*$	4.84 (256)		9×10^{-5}	H-4 → L (99)
S_8	$\pi\rightarrow\pi^*$	5.05 (246)	4.96 (250)	7×10^{-1}	H → L+2 (69)
T_1	$\pi\rightarrow\pi^*$	2.27 (547)		0×10^{0}	H → L (95)
T_2	$n\rightarrow\pi^*$	3.12 (398)		0×10^{0}	H-2 → L (89)

dx.doi.org/10.1021/jp505411r | J. Phys. Chem. A 2014, 118, 6914−6921

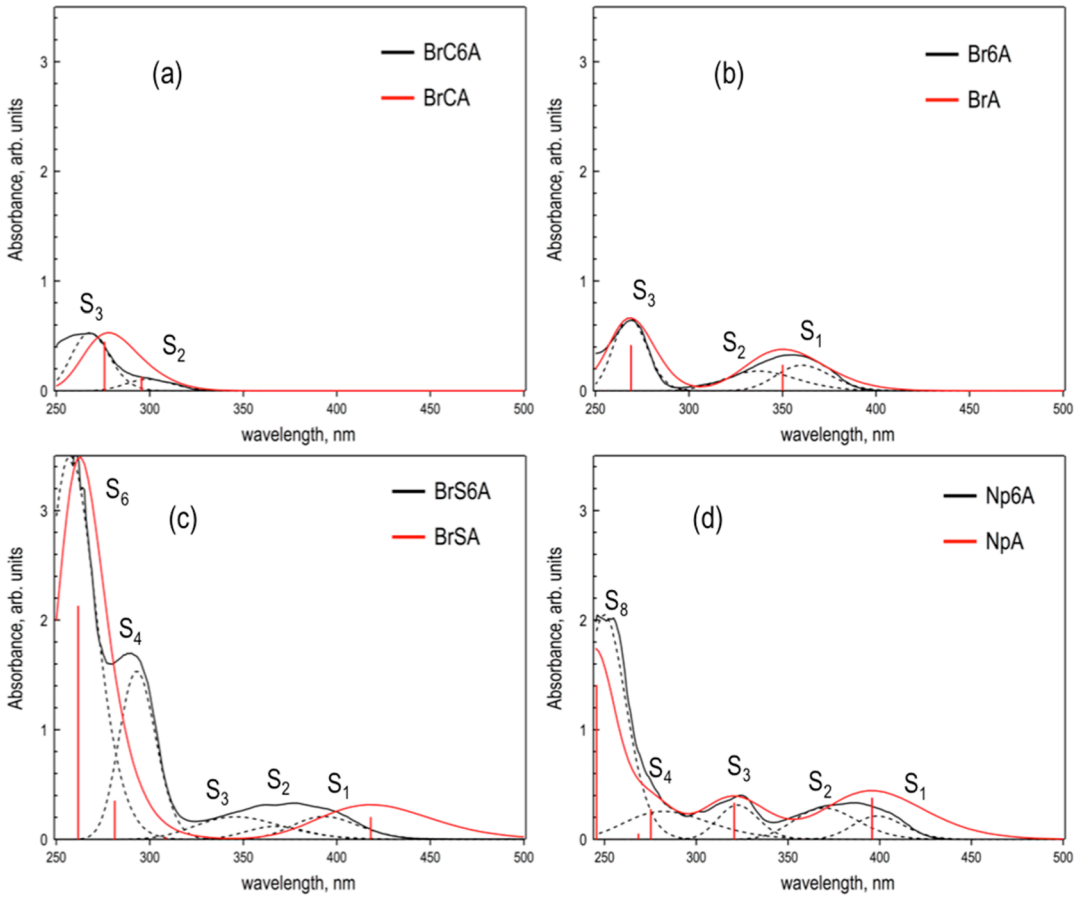

Figure 3. Measured (black) and simulated (red) absorption profiles of (a) BrC6A/BrCA, (b) Br6A/BrA, (c) BrS6A/BrSA, and (d) Np6A/NpA in chloroform solution. Dashed lines correspond to a deconvolution of the experimental spectra. Computed oscillator strengths are indicated as red vertical bars. Labeling for singlet states follows the state numeration in Table 1

Experimental spectra of Br6A (Figure 3b) exhibit two well-separated absorption bands with similar intensities (slightly higher for the band at shorter wavelengths), which can be associated with the two lowest $\pi\pi^*$ excited singlet states. The shape and width of the band at longer wavelengths suggest the contribution of more than one transition to this band. In fact, decomposition of this band reveals the presence of a less intense transition at ~330 nm that we assign to the $n\pi^*$ lowest singlet state (S_2). The computed energies to the three lowest singlet states are in very good agreement with the experimental values. TDDFT results are also able to correctly predict the relative intensities of the two absorption features. The absorption profile of BrC6A (Figure 3a) in the 250−350 nm range corresponds to the superposition of the two lowest $\pi \rightarrow \pi^*$ excitations, that is, S_2 and S_3 in Table 1. As discussed above (Figure 1), the double alkyl substitution in the BrCA molecule stabilizes the π-HOMO with respect to the BrA case, inducing a noticeable blue shift of the transition to the lowest $\pi\pi^*$ singlet. As a result, the energy gap between the S_2 and S_3 states shrinks to a few tenths of an eV and the two $\pi \rightarrow \pi^*$ absorption bands largely overlap in the spectrum for BrCA. TDDFT nicely reproduces this behavior, with higher oscillator strength for the second excitation, in fair agreement with the experiment. The BrS6A spectrum (Figure 3c) presents a rather wide band in the 325−450 nm range and two more intense bands at shorter wavelengths. Comparison between the deconvolution of the measured absorption spectrum with TDDFT calculations on BrSA suggests that the low energy band in the spectrum is due to the sum of the transitions to the lowest $^1\pi\pi^*$ state (S_1) and to the two lowest lying $^1n\pi^*$ states (S_2 and S_3). The two intense peaks at 281 and 262 nm (S_4 and S_6, respectively) correspond to higher $\pi \rightarrow \pi^*$ transitions. The lowest energy absorption band of Np6A at 350−425 nm seems to be the result of the overlap of the transitions to the S_1 ($^1\pi\pi^*$) and S_2 ($^1n\pi^*$) states (Figure 3d). We assign the peak at 321 nm to the HOMO-1 → LUMO excitation (S_3). Our results suggest that the intense band at ~250 nm in the experimental spectrum corresponds to the electronic transition from the HOMO to a higher π^* orbital, that is, LUMO+2 orbital (S_8 in Table 1). The intensity of this absorption masks the HOMO-3 → LUMO (S_4) and HOMO → LUMO+1 (S_5) transitions in the experimental spectrum. The decomposition of the experimental profile allows us to infer the position of S_4 at 282 nm, which is supported by the computed value (275 nm).

Fluorescence Spectra. The experimental photoluminescence spectra of BrC6A, Br6A, BrS6A, and Np6A recorded in chloroform solution at room temperature are shown in Figure 4. All four compounds present rather low quantum yields, and can be characterized as weak fluorescent chromophores emitting at 346, 427, 490, and 450 nm, respectively. Of the four molecules, only BrS6A exhibits sizable fluorescence efficiency with a moderate yield of 2.4% (Table 2).

TDDFT geometry optimization calculations on the excited states manifold indicate that the lowest excited singlet state of BrC6A, Br6A, and Np6A possesses $n\pi^*$ character, while in BrSA the $^1\pi\pi^*$ is the lowest adiabatic (emitting) state. In other

dx.doi.org/10.1021/jp505411r | J. Phys. Chem. A 2014, 118, 6914−6921

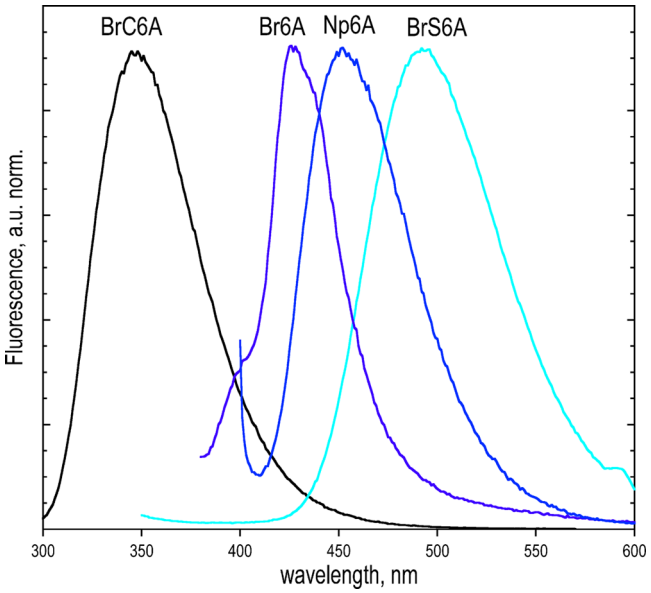

Figure 4. Normalized photoluminescence spectra of BrC6A, Br6A, BrS6A, and Np6A in chloroform solution recorded at room temperature. Trace colors correspond to the conversion of wavelengths at the band maxima to RGB values.

words, geometry relaxation following photoexcitation in BrC6A, Br6A and Np6A leads to a lowest excited singlet with nπ^* character, but the $^1\pi\pi^*/^1$nπ^* energy gap at the Franck–Condon geometry in BrSA (Figure 2) is too large to be overcome by structural rearrangement. This difference in the electronic structure of the emitting state would explain why BrS6A is much more efficient to relax back to its ground state via photoemission than the other three explored bromobenzaldehyde derivatives. Computed vertical energy gaps at the lowest excited singlet state optimized geometries are in good agreement with frequencies measured at the experimental emission peaks (Table 2). B3LYP overestimates the transition energies by 0.1–0.3 eV in Br6A, BrS6A, and Np6A. The energy obtained for BrCA presents the largest discrepancy of the studied set, with an underestimation of approximately 0.4 eV with respect to the emission peak of Br6CA. The relative energy ordering between emitters obtained experimentally is, however, well preserved in our calculations.

Optimized geometries of BrCA, BrA, BrSA, and NpA in their lowest excited singlet fairly reflect the nature of the emitting state (Table 3). Due to the nπ^* electronic character of the excited singlet, BrCA, BrA, and NpA present an increase of the C=O bond length, a decrease of the C–C distance between the aldehyde carbon atom and the conjugated ring, and an increase of ∼5 degrees in the OCC angle at the aldehyde group, with respect to the ground state structure. On the other hand, the BrSA lowest excited singlet state follows a different geometry relaxation pattern. It also experiences an increase and decrease of the C=O and C-ring bond distances, respectively, but to a lower degree, and the aldehyde angle just slightly decreases with respect to its value in the ground state structure. Optimized geometries and adiabatic excitation energies for the four studied molecules in the ground and excited singlet and triplet states can be found as Supporting Information.

Table 3. Characteristic Bond Distances (Å) and Angles (deg) for the Optimized Geometries of the BrCA, BrA, BrSA, and NpA Molecules in the Ground State (S_0) and the Lowest Excited Singlet (S_{Fl}) and Triplet (T_{Ph}) States[a]

molecule	S_0	S_{Fl}	T_{Ph}
	d_{CO}		
BrCA	1.217	1.291	1.255
BrA	1.218	1.288	1.249
BrSA	1.216	1.249	1.247
NpA	1.222	1.277	1.238
	d_{CAr}		
BrCA	1.483	1.398	1.436
BrA	1.477	1.388	1.442
BrSA	1.482	1.467	1.444
NpA	1.475	1.381	1.456
	θ_{OCC}		
BrCA	124	129	122
BrA	124	130	123
BrSA	124	122	123
NpA	127	132	127

[a] d_{CO} is the C–O distance in the carbonyl group, d_{CAr} the C–C distance between the aldehyde carbon atom and the conjugated ring, and θ_{OCC} is the O–C–C aldehyde angle.

Phosphorescence Spectra. The phosphorescence spectra of BrC6A, Br6A, and BrS6A in chloroform solution (Figure 5) have a great resemblance to the photoluminescence spectra of the corresponding crystals.[21] BrC6A exhibits the shortest emission wavelength at 450 nm (2.76 eV). The bands for

Table 2. Experimental and Computed Fluorescence and Phosphorescence Emission Energies (eV) of BrCA/BrC6A, BrA/Br6A, BrSA/BrS6A, and NpA/Np6A Molecules[a]

	fluorescence			phosphorescence		
molecule	state	ΔE_{calc}	ΔE_{exp}	state	ΔE_{calc}	ΔE_{exp}
BrCA	^{1}nπ^*	3.21	3.58	$^3\pi\pi^*$	2.52	2.76
		(3×10^{-5})	(∼0)		(5×10^{-8})	
BrA	^{1}nπ^*	3.20	2.90	$^3\pi\pi^*$	2.14	2.32
		(8×10^{-5})	(0.66)		(8×10^{-9})	
BrSA	$^1\pi\pi^*$	2.65	2.53	$^3\pi\pi^*$	1.96	2.25
		(9×10^{-2})	(2.40)		(3×10^{-8})	
NpA	^{1}nπ^*	2.91	2.76	$^3\pi\pi^*$	1.79	2.05
		(1×10^{-2})	(∼0)		(1×10^{-8})	

[a] Values in parentheses indicate computed oscillator strengths for the calculated energies and experimental fluorescence quantum yields in solution at room temperature (%).

dx.doi.org/10.1021/jp505411r | J. Phys. Chem. A 2014, 118, 6914–6921

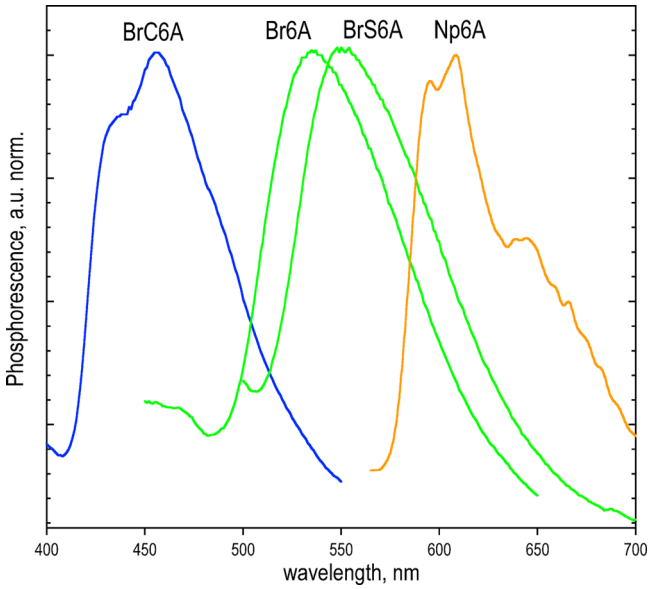

Figure 5. Normalized phosphorescence spectra of BrC6A, Br6A, BrS6A, and Np6A in chloroform solution at 77 K. Trace colors correspond to the conversion of wavelengths at the band maxima to RGB values.

Br6A and BrS6A are close to each other with maximum peaks at 535 and 550 nm (2.32 and 2.25 eV), respectively. The three bands correspond to the phosphorescence emission from the $^3\pi\pi^*$ state.

The electronic nature of the emitting triplet state is well recovered by TDDFT calculations for all four cases. The computed vertical transition energies of the four molecular models at the optimized geometry of the triplet state are in good agreement with the experimental maxima, despite the fact that B3LYP systematically underestimates the deexcitation energies by a few tenths of an eV (Table 2).

Although our calculations include relativistic effects (see the Computational Details), the results indicate that there is virtually no effective coupling between the pure singlet and triplet states. It implies that the singlet-to-triplet transition necessary to produce emission from a triplet state is rather inefficient, resulting in low phosphorescence quantum yields. This would suggest that, in addition to vibrational hindrance in the solid state, the presence of a Br atom of the neighboring molecule close to the aldehyde group is crucial in order to reach the much larger efficiencies recorded for the crystal compared to the phosphorescence in solution. Further studies on this aspect are currently being developed in our groups.

The lowest triplet state in all four molecules corresponds to a $\pi\pi^*$ state and geometry relaxation on the triplet manifold (Table 3) follows similar trends as the ones described previously for the optimized $^1\pi\pi^*$ state in BrSA.

5. CONCLUSIONS

In this work we have undertaken the characterization of the electronic structure of the low-lying $n\pi^*$ and $\pi\pi^*$ states of benzaldehyde derivatives by means of their molecular orbital energy diagrams. We have applied this scheme to the description of the BrCA, BrA, BrSA, and NpA 4-bromobenzaldehyde derivatives as molecular models for the computational study of the molecular analogues with side hydrocarbon chains, that is, BrC6A, Br6A, BrS6A, and Np6A for which absorption, fluorescence, and phosphorescence spectra in chloroform solution have been recorded.

The main features of the absorption profiles have been discussed and interpreted by means of TDDFT calculations. We have been able to assign all experimental peaks of the spectra to electronic transitions from valence electrons to low-lying empty molecular orbitals. We have also presented and analyzed the experimental fluorescence and phosphorescence emission spectra in solution for the four chromophores. Our calculations suggest that Br6A, BrC6A, and Np6A emit from the lowest $^1n\pi^*$ state, while the emitting singlet in BrS6A is of $\pi\pi^*$ character. This finding is in agreement with the higher photoluminescence efficiency measured for BrS6A.

Compared to the high quantum yields observed in the solid state, the studied molecules present very low phosphorescence intensities in solution. The presence of a Br atom close to the aldehyde group in the crystal structure seems thus to be the main reason for the different behavior observed in the solid state. This conclusion is in line with the previous studies performed on the crystal structures.[21] In a forthcoming study, we will focus our efforts to unravel this and other questions regarding the mechanisms dominating the singular photophysical properties in the solid state of Br6A, Br6CA, Br6SA, and Np6A chromophores.

■ ASSOCIATED CONTENT

Supporting Information

A figure showing the adiabatic relative energies of the lowest states for all studied molecules; vertical excitation energies to low-lying states of BrA computed with TZ2P and ATZ2P basis sets; optimized coordinates for BrCA, BrA, BrSA, and NpA; vertical transition energies obtained with LR-COSMO, LR-PCM, and SS-PCM solvation models; fluorescence and phosphorescence emission energies computed with LR-COSMO and SS-PCM models. This material is available free of charge via the Internet at http://pubs.acs.org.

■ AUTHOR INFORMATION

Corresponding Author

*E-mail: david.casanova@ehu.es.

Notes

The authors declare no competing financial interest.

■ ACKNOWLEDGMENTS

The authors want to thank Professor J. M. Bofill for fruitful discussions and valuable insights. Financial support for this work was provided by the Spanish *Ministerio de Economía y Competitividad* through Project CTQ2011-23862-C02-02/BQU and the *Generalitat de Catalunya* through Project 2009SGR-1459. The computing resources used were generously made available at the Centre de Computació de Catalunya (CESCA) through a grant provided by Fundació Catalana per a la Recerca (FCR) and Universitat de Barcelona. D.C. gratefully acknowledges the IKERBASQUE, Basque Foundation for Science, for financial support.

■ REFERENCES

(1) Beaujuge, P. M.; Reynolds, J. R. Color Control in Π-Conjugated Organic Polymers for Use in Electrochromic Devices. *Chem. Rev.* **2010**, *110* (1), 268−320.

(2) Forrest, S. R.; Thompson, M. E. Introduction: Organic Electronics and Optoelectronics. *Chem. Rev.* **2007**, *107* (4), 923−925.

(3) McCulloch, I. Organic Electronics. *Adv. Mater.* **2013**, *25* (13), 1811−1812.
(4) Hu, W.; Bao, Z.; Muellen, K. Themed Issue on "Organic Optoelectronic Materials". *J. Mater. Chem.* **2012**, *22* (10), 4134−4135.
(5) Caironi, M.; Anthopoulos, T. D.; Noh, Y.-Y.; Zaumseil, J. Organic and Hybrid Materials for Flexible Electronics. *Adv. Mater.* **2013**, *25* (31), 4208−4209.
(6) Hu, W.; Bai, F.; Gong, X.; Zhan, X.; Fu, H.; Bjornholm, T. *Organic Optoelectronics*; Wiley-VCH: 2013.
(7) Flamigni, L.; Barbieri, A.; Sabatini, C.; Ventura, B.; Barigelletti, F. Photochemistry and Photophysics of Coordination Compounds: Iridium. *Top. Curr. Chem.* **2007**, *281*, 143−203.
(8) Yersin, H. *Highly Efficient Oleds with Phosphorescent Materials*; Wiley-VCH Verlag GmbH & Co. KGaA: Weinheim, Germany, 2008.
(9) Berger, M.; Goldblatt, I. L.; Steel, C. Photochemistry of Benzaldehyde. *J. Am. Chem. Soc.* **1973**, *95* (6), 1717−1725.
(10) Iguchi, K. Lifetime of Phosphorescence of Substituted Naphthalenes. *J. Chem. Phys.* **1959**, *30* (1), 319−320.
(11) Terenin, A.; Ermolaev, V. Sensitized Phosphorescence in Organic Solutions at Low Temperature. Energy Transfer between Triplet States. *Trans. Faraday Soc.* **1956**, *52* (0), 1042−1052.
(12) El-Sayed, M. A. Triplet State. Its Radiative and Nonradiative Properties. *Acc. Chem. Res.* **1968**, *1* (1), 8−16.
(13) Kasha, M. Phosphorescence and the Role of the Triplet State in the Electronic Excitation of Complex Molecules. *Chem. Rev.* **1947**, *41* (2), 401−419.
(14) Koziar, J. C.; Cowan, D. O. Photochemical Heavy-Atom Effects. *Acc. Chem. Res.* **1978**, *11* (9), 334−341.
(15) Turro, N. J. *Modern Molecular Photochemistry*; University Science Books: 1991.
(16) McGlynn, S. P.; Azumi, T.; Kasha, M. External Heavy-Atom Spin—Orbital Coupling Effect. V. Absorption Studies of Triplet States. *J. Chem. Phys.* **1964**, *40* (2), 507−515.
(17) El-Sayed, M. A.; Pavlopoulos, T. Intramolecular Heavy-Atom Effect on the Polarization of Naphthalene Phosphorescence. *J. Chem. Phys.* **1963**, *39* (7), 1899−1900.
(18) Lower, S. K.; El-Sayed, M. A. The Triplet State and Molecular Electronic Processes in Organic Molecules. *Chem. Rev.* **1966**, *66* (2), 199−241.
(19) Borkman, R. F.; Kearns, D. R. Heavy-Atom and Substituent Effects on S—T Transitions of Halogenated Carbonyl Compounds. *J. Chem. Phys.* **1967**, *46* (6), 2333−2341.
(20) Kasha, M. Collisional Perturbation of Spin-Orbital Coupling and the Mechanism of Fluorescence Quenching. A Visual Demonstration of the Perturbation. *J. Chem. Phys.* **1952**, *20* (1), 71−74.
(21) Bolton, O.; Lee, K.; Kim, H.-J.; Lin, K. Y.; Kim, J. Activating Efficient Phosphorescence from Purely Organic Materials by Crystal Design. *Nat. Chem.* **2011**, *3* (3), 205−210.
(22) Charaf-Eddin, A.; Planchat, A.; Mennucci, B.; Adamo, C.; Jacquemin, D. Choosing a Functional for Computing Absorption and Fluorescence Band Shapes with TD-DFT. *J. Chem. Theory Comput.* **2013**, *9* (6), 2749−2760.
(23) Jacquemin, D.; Wathelet, V.; Perpète, E. A.; Adamo, C. Extensive TD-DFT Benchmark: Singlet-Excited States of Organic Molecules. *J. Chem. Theory Comput.* **2009**, *5* (9), 2420−2435.
(24) Guido, C. A.; Knecht, S.; Kongsted, J.; Mennucci, B. Benchmarking Time-Dependent Density Functional Theory for Excited State Geometries of Organic Molecules in Gas-Phase and in Solution. *J. Chem. Theory Comput.* **2013**, *9* (5), 2209−2220.
(25) Goerigk, L.; Grimme, S. Assessment of TD-DFT Methods and of Various Spin Scaled CIS(D) and CC2 Versions for the Treatment of Low-Lying Valence Excitations of Large Organic Dyes. *J. Chem. Phys.* **2010**, *132* (18), 184103.
(26) Guillaumont, D.; Nakamura, S. Calculation of the Absorption Wavelength of Dyes Using Time-Dependent Density-Functional Theory (TD-DFT). *Dyes Pigm.* **2000**, *46* (2), 85−92.
(27) Laurent, A. D.; Adamo, C.; Jacquemin, D. Dye Chemistry with Time-Dependent Density Functional Theory. *Phys. Chem. Chem. Phys.* **2014**, *16* (28), 14334−14356.
(28) Cramer, C. J.; Truhlar, D. G. Implicit Solvation Models: Equilibria, Structure, Spectra, and Dynamics. *Chem. Rev.* **1999**, *99* (8), 2161−2200.
(29) Tomasi, J.; Mennucci, B.; Cammi, R. Quantum Mechanical Continuum Solvation Models. *Chem. Rev.* **2005**, *105* (8), 2999−3094.
(30) Schäfer, A.; Horn, H.; Ahlrichs, R. Fully Optimized Contracted Gaussian Basis Sets for Atoms Li to Kr. *J. Chem. Phys.* **1992**, *97* (4), 2571−2577.
(31) Shao, Y.; Molnar, L. F.; Jung, Y.; Kussmann, J.; Ochsenfeld, C.; Brown, S. T.; Gilbert, A. T. B.; Slipchenko, L. V.; Levchenko, S. V.; O'Neill, D. P.; et al. Advances in Methods and Algorithms in a Modern Quantum Chemistry Program Package. *Phys. Chem. Chem. Phys.* **2006**, *8* (27), 3172−3191.
(32) Baerends, E.J.; Ziegler, T.; ; Autschbach, J.; Bashford, D.; A. Bérces; Bickelhaupt, F.M.; Bo, C.; Boerrigter, P.M.; Cavallo, L.; Chong, D.P. et al. *Theoretical Chemistry*; ADF2012, SCM; Vrije Universiteit: Amsterdam, The Netherlands, 2012.
(33) te Velde, G.; Bickelhaupt, F. M.; Baerends, E. J.; Fonseca Guerra, C.; van Gisbergen, S. J. A.; Snijders, J. G.; Ziegler, T. Chemistry with ADF. *J. Comput. Chem.* **2001**, *22* (9), 931−967.
(34) van Gisbergen, S. J. A.; Snijders, J. G.; Baerends, E. J. Implementation of Time-Dependent Density Functional Response Equations. *Comput. Phys. Commun.* **1999**, *118* (2−3), 119−138.
(35) van Lenthe, E.; Baerends, E. J.; Snijders, J. G. Relativistic Total Energy Using Regular Approximations. *J. Chem. Phys.* **1994**, *101* (11), 9783−9792.
(36) Wang, F.; Ziegler, T. A Simplified Relativistic Time-Dependent Density-Functional Theory Formalism for the Calculations of Excitation Energies Including Spin-Orbit Coupling Effect. *J. Chem. Phys.* **2005**, *123* (15), 154102.
(37) Van Lenthe, E.; Baerends, E. J. Optimized Slater-Type Basis Sets for the Elements 1−118. *J. Comput. Chem.* **2003**, *24* (9), 1142−1156.
(38) Pye, C. C.; Ziegler, T. An Implementation of the Conductor-like Screening Model of Solvation within the Amsterdam Density Functional Package. *Theor. Chem. Acc.* **1999**, *101* (6), 396−408.
(39) Klamt, A.; Schuurmann, G. COSMO: A New Approach to Dielectric Screening in Solvents with Explicit Expressions for the Screening Energy and Its Gradient. *J. Chem. Soc. Perkin Trans. 2* **1993**, No. 5, 799−805.
(40) Cammi, R.; Mennucci, B. Linear Response Theory for the Polarizable Continuum Model. *J. Chem. Phys.* **1999**, *110* (20), 9877−9886.
(41) Cossi, M.; Barone, V. Time-Dependent Density Functional Theory for Molecules in Liquid Solutions. *J. Chem. Phys.* **2001**, *115* (10), 4708−4717.
(42) Improta, R.; Barone, V.; Scalmani, G.; Frisch, M. J. A State-Specific Polarizable Continuum Model Time Dependent Density Functional Theory Method for Excited State Calculations in Solution. *J. Chem. Phys.* **2006**, *125* (5), 054103.
(43) Improta, R.; Scalmani, G.; Frisch, M. J.; Barone, V. Toward Effective and Reliable Fluorescence Energies in Solution by a New State Specific Polarizable Continuum Model Time Dependent Density Functional Theory Approach. *J. Chem. Phys.* **2007**, *127* (7), 074504.
(44) Mennucci, B. Polarizable Continuum Model. *WIREs* **2012**, *2* (3), 386−404.
(45) Frisch, M. J.; Trucks, G. W.; Schlegel, H. B.; Scuseria, G. E.; Robb, M. A.; Cheeseman, J. R.; Scalmani, G.; Barone, V.; Mennucci, B.; Petersson, G. A. et al. *Gaussian 09*, Gaussian, Inc.: Wallingford, CT, USA, 2009.
(46) Weigend, F.; Ahlrichs, R. Balanced Basis Sets of Split Valence, Triple Zeta Valence and Quadruple Zeta Valence Quality for H to Rn: Design and Assessment of Accuracy. *Phys. Chem. Chem. Phys.* **2005**, *7* (18), 3297−3305.
(47) Chong, D. P. Augmenting Basis Set for Time-Dependent Density Functional Theory Calculation of Excitation Energies: Slater-Type Orbitals for Hydrogen to Krypton. *Mol. Phys.* **2005**, *103* (6−8), 749−761.